Device-Package Interaction and Gate Driver Layout Analysis in SiC MOSFET Power Modules for More Electric Aircraft Motor Drive Applications

Shane O'Donnell[1,2], Laurence Egan[1], Vincent Walsh[1], Pat Wheeler[2] and Alberto Castellazzi[2]

[1] MICROSEMI CORPORATION
Gort Road Business Park
Ennis, Co. Clare, Ireland
Tel: +353 (0) 65 68 40044
sodonnell@microsemi.com
http://www.microsemi.com

[2] UNIVERSITY OF NOTTINGHAM
University Park
Nottingham NG7 2RD, UK
Tel: +44 (0) 115 951 5151
http://www.nottingham.ac.uk

Acknowledgements

The authors wish to acknowledge the support provided by the Microsemi Integrated Power Solutions™ team.

Keywords

«Aerospace», «Device characterisation», «Intelligent Power Module (IPM)», «Measurement», «MOSFET», «Power semiconductor device», «Silicon Carbide (SiC)», «Wide bandgap devices».

Abstract

This paper presents measurements and comparison analysis of 1200 V SiC MOSFET gate drive signals in two different integrated power solutions designed for More Electric Aircraft motor drive applications. The modules are designed to accommodate a 540 V high voltage DC bus and have a maximum output phase current of 25 A peak. Both modules comprise of typical three-phase inverter bridge configurations, with 40 mΩ MOSFETs and 20 A anti-parallel diodes. However, their gate drivers, printed circuit board layouts and substrate designs are different and the effect these elements have on the performance is presented. The results illustrate that gate resistances, package interactions and PCB layout can have a major effect on performance while variations in switching frequency, from 10 kHz to 50 kHz, and a reduction in dead-time, from 500 ns to 375 ns, have negligible impacts.

Introduction

In modern aircraft, the use of Insulated Gate Bipolar Transistor (IGBT) technology is currently the favoured approach in the design of power converters used for driving electrical motors. These devices meet the fundamental requirements for the application and as they have been widely used for many years, their characteristics are well known and their reliability is very much established.

Wide bandgap semiconductor materials, however, such as silicon carbide (SiC), have properties which offer significant advantages over silicon (Si) such as improved power density, lower losses and operation at higher junction temperatures [1], [2], [3], [4], [5]. In applications such as commercial aviation, where size and weight are influencing factors, the emergence of SiC Metal Oxide Semiconductor Field Effect Transistors (MOSFETs) as alternatives to Si IGBTs has been extremely beneficial [6], [7], [8], [9] as power electronics become more essential in the More Electric Aircraft (MEA) development [10]. The use of SiC MOSFETs in high-reliability applications, however, has been somewhat limited due their relative immaturity and lack of flight heritage in critical applications, such as flight control actuation systems. Power modules designed for such applications are expected to last for up to 150,000 flight hours of operation and therefore the life-time of individual components must far exceed this

requirement. With inappropriate operation of the SiC MOSFET drive circuitry the performance and long-term reliability of the unit may be compromised.

This paper presents two different inverter modules designed for motor control applications. Their designs are compared and measurements are provided to characterise the SiC MOSFET gate drive signals. Both designs accommodate a high voltage DC supply of 540 V, use the same 1200 V, 40 mΩ SiC MOSFETs [11] and 20 A anti-parallel Schottky Barrier Diodes (SBDs) [12], and drive an output current of 25A into an inductive-resistive load for this analysis. This current is the limit of operation of these 5 kVA modules, which typically operate with a 12.5 A output. The same power supplies and loads are used for all measurements to minimise equipment and test setup variability. The results provide insights into the effects that different circuits and layout configurations can have in the gate drive of SiC MOSFETs.

Integrated Power Solutions Modules

The integrated power solutions modules used in this study have been designed for similar applications but have different integration schemes into higher level assemblies. The two modules are shown in Figure 1 below.

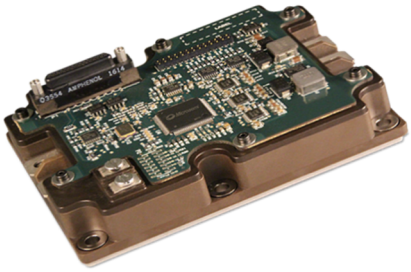

Figure 1a: 5 kVA Power Core Module (PCM) demonstrator.

Figure 1b: 5 kVA High Power Electronics Module (HPEM) demonstrator.

These modules are designed for use in More Electric Aircraft applications to drive electrical motors in application areas such as primary and secondary flight control, landing gear and braking systems. They may be integrated into a complete Power Drive Electronics architecture as shown below in Figure 2.

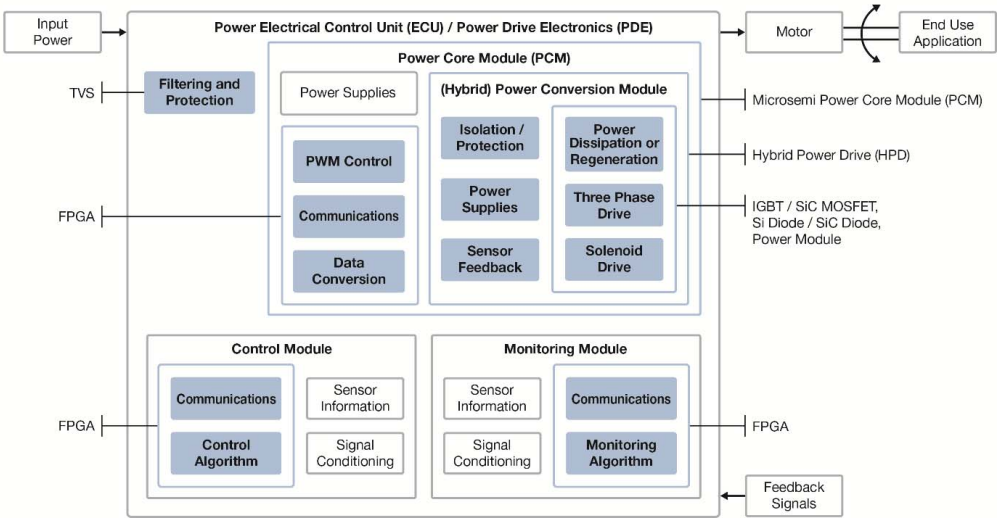

Figure 2: Aviation Intelligent Power Electrical Control System

The PCM and HPEM demonstrators used in this study comprise of the following sub-systems:

- Substrate assemblies, containing the SiC MOSFETs and anti-parallel SiC SBDs.

- Printed circuit board assemblies (PCBAs) containing the gate driver circuitry, isolated power supplies and conditioning circuitry for measuring output current.

- The PCM contains a telemetry PCBA containing 12-bit analog-to-digital converters (ADCs) and a Microsemi ProAsic3 Field Programmable Gate Array (FPGA) [13], which communicates with the ADCs and with an external master controller board or special test equipment (STE). This is used to verify the current measurements recorded with the oscilloscope.

- The HPEM driver board contains 12-bit ADCs with a serial peripheral interface (SPI). An external controller, namely a Microsemi IGLOO2 development kit [14], is used to communicate with the HPEM and extract telemetry information for analysis. Similar to the PCM telemetry board, this interface is used to verify the measured results.

- The high voltage (HV) DC is connected to the PCM through the screw terminals shown on the left side of Figure 1a, while the connections to the motor are on the right side. Therefore, the PCM can be easily replaced in the next level assembly, if required.

- In the HPEM design, the HVDC is connected via the pins in the centre of the unit as shown in Figure 1b, and the motor connections are via the pins shown towards the top of the image. These pins are soldered to the next level assembly so removal and replacement is more difficult than with the PCM.

A summary comparison of the key features and differences between the two designs, in addition to the difference in location of the HVDC and motor output connections, is shown in Table 1 below.

Table 1: Comparison of PCM and HPEM

	PCM	HPEM
Nominal high voltage supply	540 VDC	540 VDC
Power rating (540V)	5 kVA	5 kVA
Maximum peak output current	25 A	25 A
Nominal peak output current	12.5 A	12.5 A
Motor drive architecture	Three-phase half-bridge	Three-phase half-bridge
Dimensions (W x D x H)	105 mm x 85 mm x 30 mm	92 mm x 82 mm x 19 mm
Dimensions without telemetry PCBA	105 mm x 85 mm x 25 mm	Not applicable
Connection to next level assembly	Screw terminals	Solderable pins

In addition to the differences in the circuit layout, there were also some notable differences in the gate drive as shown in Table 2 below. The same MOSFETs and diode part numbers are used in the switching circuitry.

Table 2: Gate Drive Comparisons

PCM	HPEM
Infineon 1EDI60I12AF gate drivers [15]	Texas Instruments ISO5852 gate drivers [16]
10 Ω ohms gate drive resistors on driver PCBA	10 Ω gate drive resistors on driver PCBA
5 Ω ohms gate drive resistors on substrate assembly	No gate resistors on substrate assembly

The measurements presented in this paper illustrate the effect of these differences.

Experimental Setup

The test setup for the PCM measurements is shown in Figure 3. The STE interface PCBA is used only for testing the PCM while the IGLOO2 evaluation board is used exclusively for the HPEM testing. The HPEM test setup is identical to Figure 3 except the PCM is replaced by the HPEM.

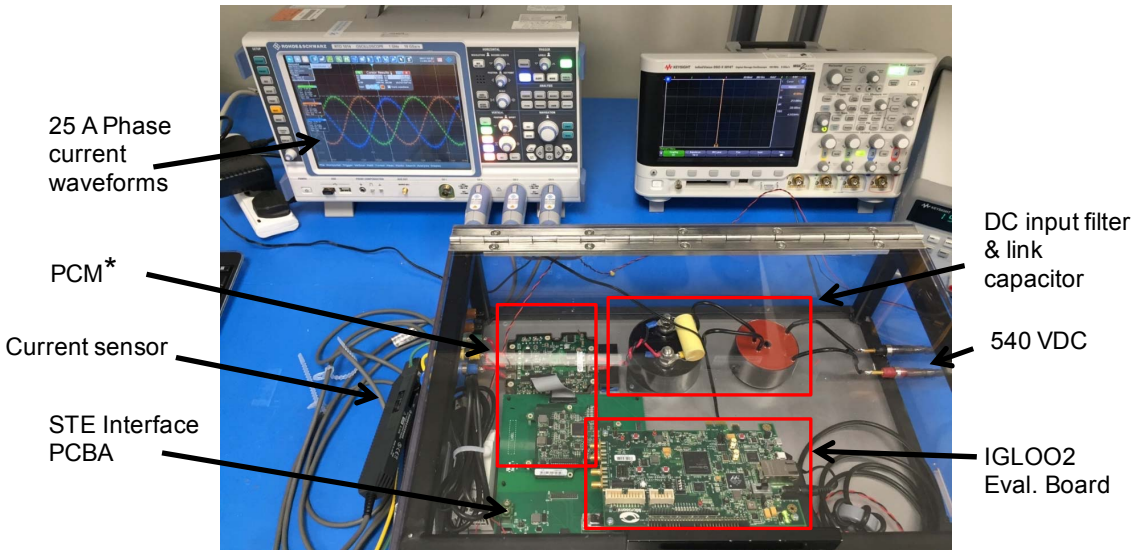

Figure 3: PCM Test Setup

* The PCM telemetry board is removed from the assembly and placed on the STE interface PCBA.

The output current is measured using hall-effect sensors on the PCM and shunt resistors on the HPEM. Using the on-board ADCs, these measurements are digitised and transmitted serially to an external PC. The output currents are then re-constructed and compared with the current measurements obtained using oscilloscope current probes to verify correction operation of the unit and equipment.

The high voltage supply is set at 540 V and the load used for the testing comprises of a 2.5 mH inductor and 2.2 Ω resistor per output phase. The output frequency is set at 400 Hz and with a modulation index of 0.629, the output current is 25 A peak. The PWM frequency is initially set at 10 kHz, which is the

default value for normal operation, but varied through the testing as presented later in this paper. All measurements were taken at a room temperature of 22 °C.

The three-phase output currents for both modules are displayed in Figure 4 below. The graphs illustrate the nominal peak output current of 25 A.

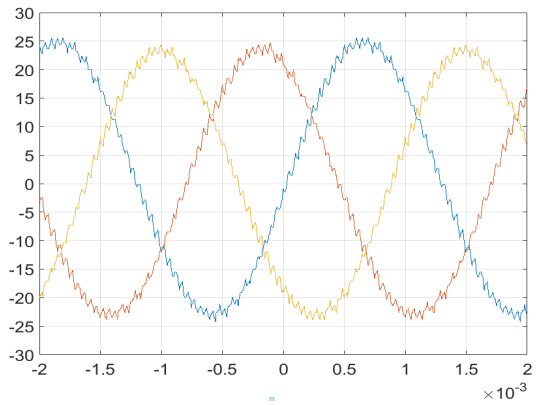

Figure 4a: PCM 3-phase output currents

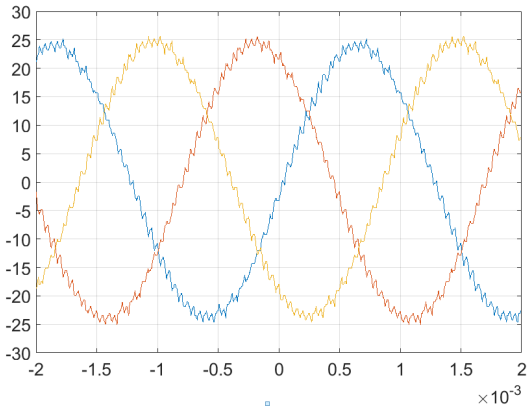

Figure 4b: HPEM 3-phase output currents

Test Results

Baseline Measurements

The baseline measurements, shown in Figure 5 to Figure 8 below, form a benchmark from which to assess the effects of variations in switching frequency (F_{SW}) and dead-time. These 2 parameters were set at 10 kHz and 500 ns respectively initially. Figure 5 presents the gate-source (V_{GS}) switching waveforms for one of the phases, designated phase 'U', over a 2.4 ms duration. The measured sinusoidal output phase currents are also shown, illustrating the variation of the 25 A (peak) signal over this time. No filtering of the measurement signals has been applied to the data.

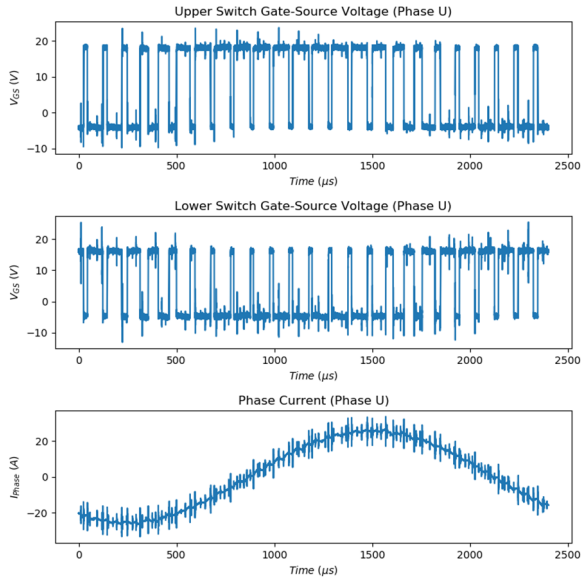

Figure 5a: PCM Phase U MOSFET switching and output current

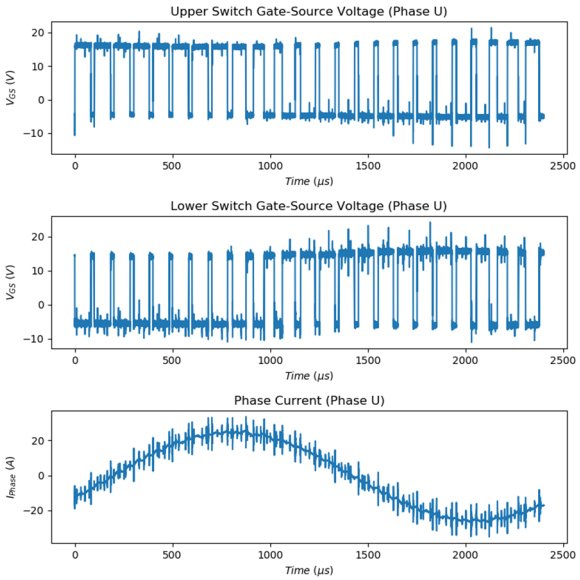

Figure 5b: HPEM Phase U MOSFET switching and output current

Further analysing these measurements shows the variation in the gate-source voltage as the output current transitions between negative and positive cycles. Figure 6a displays the gate-source voltage signals on the PCM upper and lower switches with the signals triggered on the switch-on of the lower

FET, while Figure 6b shows the corresponding signals on the HPEM. The output phase current is negative during this switching.

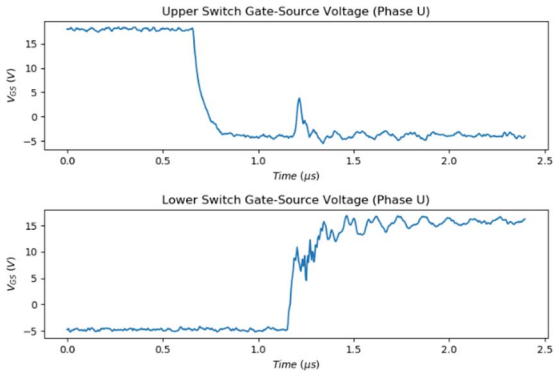

Figure 6a: PCM Phase U MOSFET switching, lower switch turn-on, negative output current

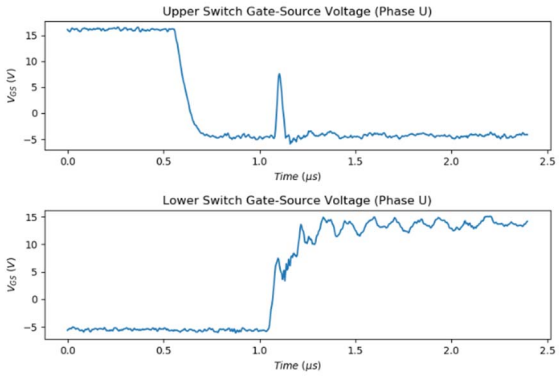

Figure 6b: HPEM Phase U MOSFET switching, lower switch turn-on, negative output current

As the upper switch turns off, the lower switch turns on after the programmed 500 ns dead-time. At this point, the miller effect is evident, resulting in a temporary reduction of the gate-source voltage on the lower switch and a corresponding positive spike in the gate-source voltage of the upper switch. As expected, the PCM and HPEM waveforms are similar. However, the magnitude of the spike in the upper FET, as the lower FET switches on, is significantly larger in the HPEM.

When the output current is positive, similar effects are seen as the upper switch turns off, with a temporary slight increase in the gate-source voltage resulting in a negative spike on the bottom V_{GS}. These measurements are shown in Figure 7.

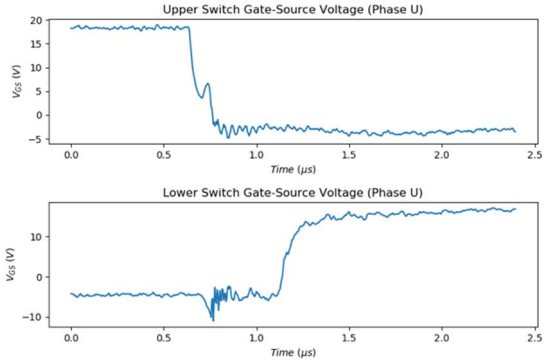

Figure 7a: PCM Phase U MOSFET switching, lower switch turn-on, positive output current

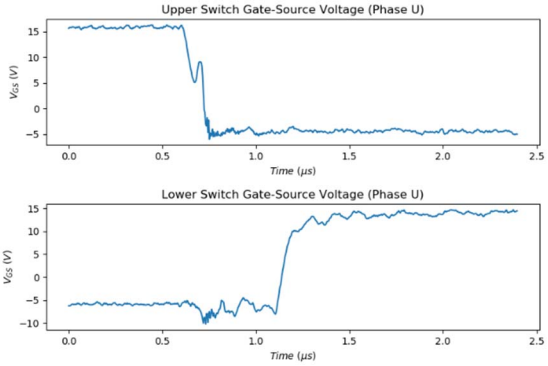

Figure 7b: HPEM Phase U MOSFET switching, lower switch turn-on, positive output current

There is little difference in the gate-source voltage measurements when the lower switch is off and the upper switch turns on as shown in Figure 8. Again, the miller effect is evident but the impact is lower than shown in Figure 6.

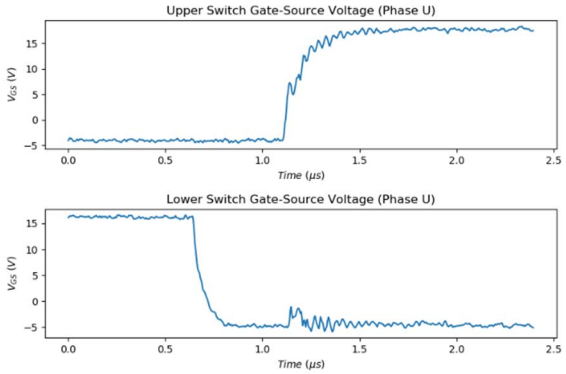

Figure 8a: PCM Phase U MOSFET, upper switch turn-on, positive output current.

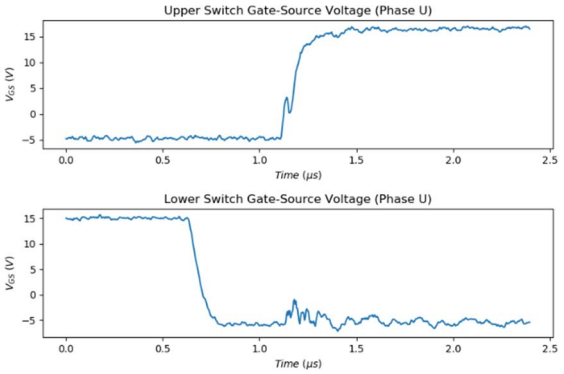

Figure 8b: HPEM Phase U MOSFET, upper switch turn-on, positive output current.

Variation in Switching Frequency

To illustrate the effect, if any, an increase in switching frequency has on the signals displayed in Figure 6, F_{SW} was increased to 20 kHz and 50 kHz. The results are shown in Figure 9 and Figure 10. These are similar to the 10 kHz results plotted in Figure 6.

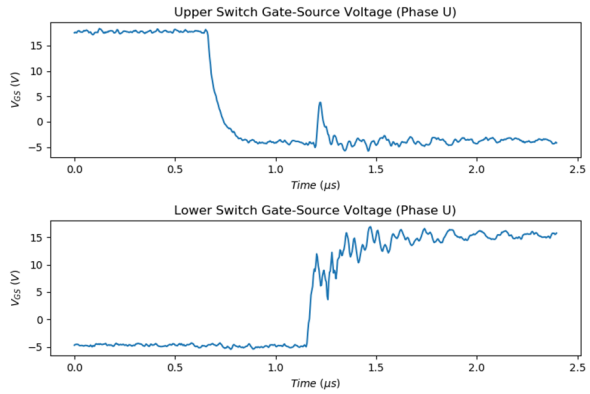

Figure 9a: PCM Phase U MOSFET 20 kHz switching, lower switch turn-on, negative output current.

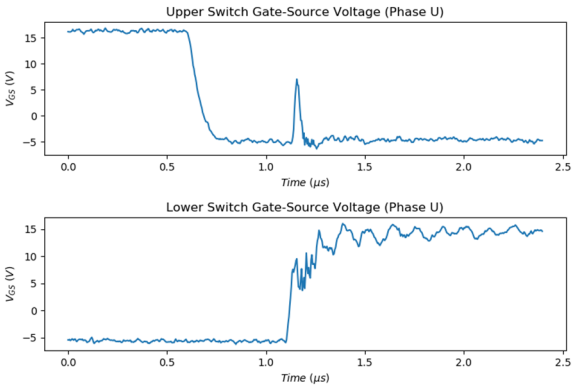

Figure 9b: HPEM Phase U MOSFET 20 kHz switching, lower switch turn-on, negative output current.

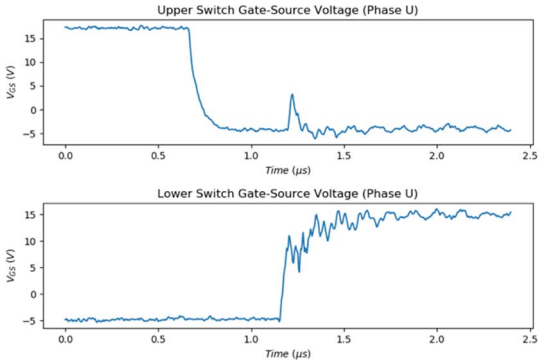

Figure 10a: PCM Phase U MOSFET 50 kHz switching, lower switch turn-on, negative output current.

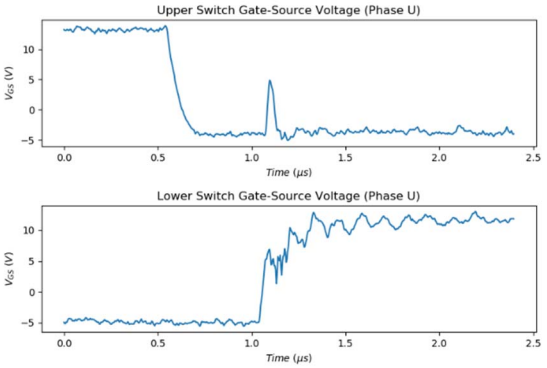

Figure 10b: HPEM Phase U MOSFET 50 kHz switching, lower switch turn-on, negative output current.

The results illustrate that increasing the switching frequency has no noticeable effect on the gate-source switch characteristics.

Variation in Dead-Time

To characterise the effect of a dead-time reduction on the modules, measurements were taken with an adjusted dead-time value of 375 ns. Similar to the frequency variation outcome, the plots presented in Figure 11 illustrate that this has negligible impact on the V_{GS} signals.

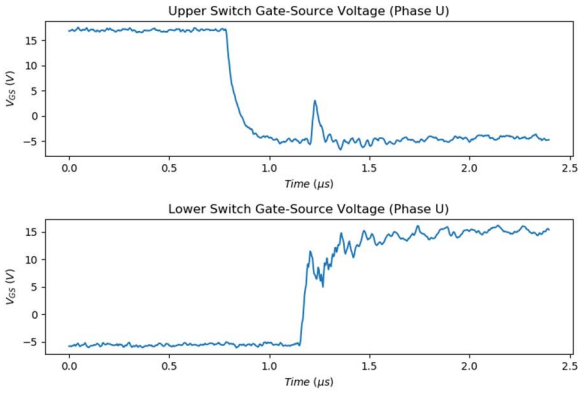

Figure 11a: PCM Phase U MOSFET 10 kHz switching, 375 ns dead-time, negative output current.

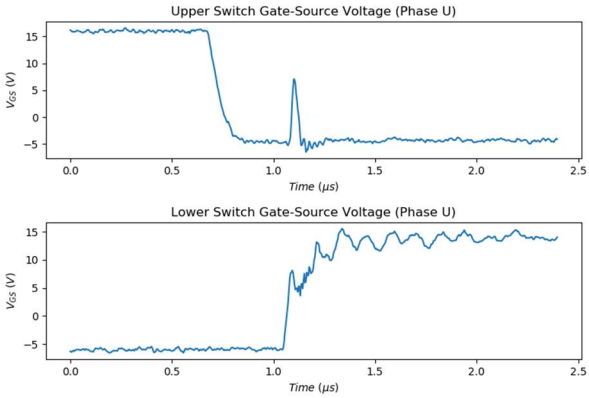

Figure 11b: HPEM Phase U MOSFET 10 kHz switching, 375 ns dead-time, negative output current.

Gate-Source Voltage Analysis

Further analysis was performed on the V_{GS} signals to understand the difference in amplitudes of the voltage spikes seen on the upper MOSFETs in the PCM and HPEM modules. As the lower MOSFET switched on, its drain-source voltage (V_{DS}) was measured. This data, with the corresponding upper switch V_{GS} measurements, is shown in Figure 12.

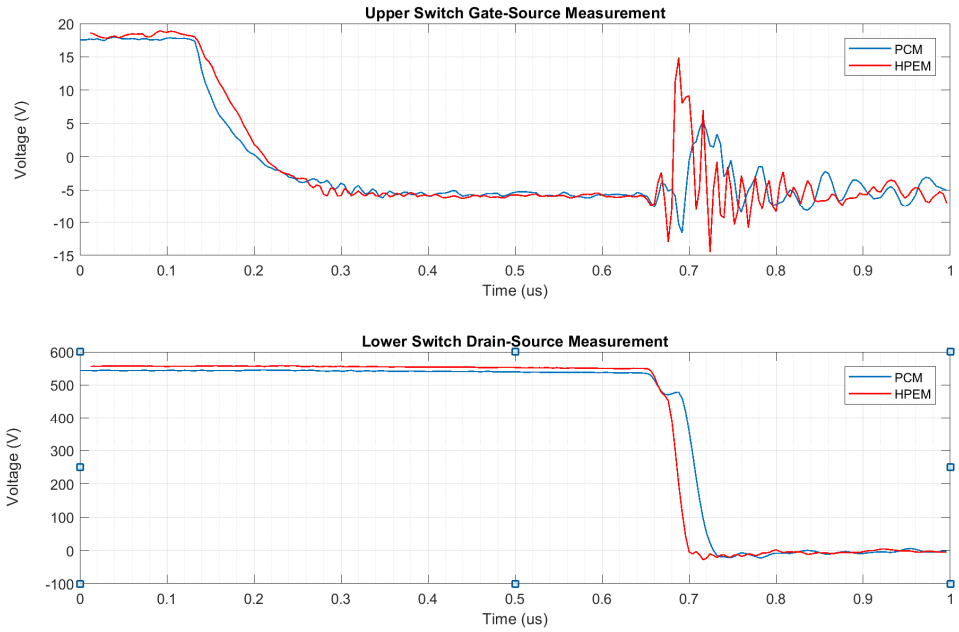

Figure 12: Comparison of PCM and HPEM V_{GS} and V_{DS} signals.

The HPEM V_{DS} displays a 40% faster switching time over the PCM. To complete the analysis on these units, the gate resistance of the HPEM was increased from 10 Ω to 15 Ω, thereby equaling the total gate

resistance in the PCM. This had a positive effect in slowing down the V_{DS} switching, but the amplitude of the voltage overshoot increased marginally as shown in Figure 13.

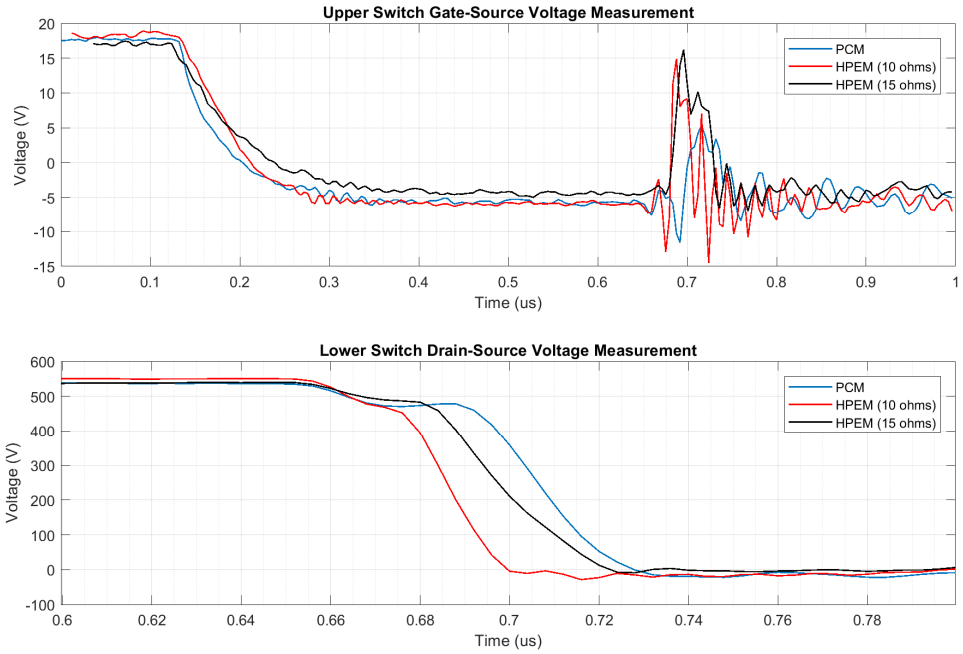

Figure 13: Comparison of PCM and HPEM 10 Ω and 15 Ω V_{GS} and V_{DS} signals.

Conclusion

This paper presents two different power modules designed for motor drive applications in More Electric Aircraft and compares the gate-source drive signals of the SiC MOSFETs used in the output power stages. A number of variables, namely switching frequency, dead-time and gate resistance were modified to determine their effect. When the output current is negative, this study concludes that the large voltage spike, which appears on the upper MOSFET as the lower MOSFET switches on, is more noticeable in the HPEM design and there is a risk that this voltage spike may result in a brief turn-on of the former resulting in a possible momentary shoot-through condition. Varying the switching frequency and dead-time had negligible effect on the measured V_{GS} data. Increasing the gate drive resistance from 10 Ω to 15 Ω on the HPEM resulted in a reduced switch-on time of the lower MOSFET but the amplitude of the voltage spike marginally increased. The modules are integrated power solutions containing substrate and printed circuit board assemblies with multiple circuit elements such as local power supplies, MOSFET/IGBT drivers and monitoring circuitry. The results from this study indicate that these circuit elements, together with the PCB and substrate layouts, are the dominant factors in the variation of the gate drive signals. One of the advantages of wide bandgap semiconductors is their ability to operate at higher frequencies and the measurements presented in this paper illustrate the switching frequency of these modules can be increased from 10 kHz to 50 kHz with a negligible impact on the gate-drive performance. This results in increased application usage, beyond actuation, into areas such as power distribution within a More Electric Aircraft.

There is a future need to validate the robustness of the design with SiC MOSFETs from different device manufacturers and the results presented in this paper indicate that sufficient control can be implemented to meet this requirement.

References

[1] J. Millan, P. Godignon, X. Perpinya, A. Perez-Tomas, and J. Rebollo,"A Survey of Wide Band Gap Power Semiconductor Devices," IEEE Transactions on Power Electronics., Vol. 29, No. 5, pp. 2155–2163, May 2014.

[2] J. Biela, M. Schweizer, S. Waffler, B. Wrzecionko, and J. W. Kolar, "SiC vs. Si—Evaluation of potentials for performance improvement of Inverter and DC-DC Converter Systems by SiC Power Semiconductors", IEEE Transactions on Industrial Electronics, Vol. 58, No. 7, July 2011.

[3] A. Elasser and T.P. Chow, "Silicon Carbide Benefits and Advantages for Power Electronics Circuits and Systems", Proc. IEEE, Vol. 90, pp. 969-986, 2002.

[4] Lixing Fu ; Xuan Zhang ; Scott, M. ; Chengcheng Yao ; Jin Wang, "The evaluation and application of wide bandgap power devices", Transportation Electrification Asia-Pacific (ITEC Asia-Pacific), 2014 IEEE Conference and Expo, pp. 1-5, Aug.-Sept. 2014.

[5] Haihong Qin ; Bin Zhao ; Xin Nie ; Jiaopu Wen ; Yangguang Yan, "Overview of SiC power devices and its applications in power electronic converters", 8th IEEE Conference on Industrial Electronics and Applications (ICIEA), pp. 466-471, June 2013.

[6] Dimitrijev, S.; Han, J. ; Haasmann, D. ; Moghadam, H.A. ; Aminbeidokhti, A. "Power-switching applications beyond silicon: The status and future prospects of SiC and GaN devices", 29th International Conference on Microelectronics Proceedings - MIEL, pp. 43-46, May 2014.

[7] Ong, A. ; Carr, J. ; Balda, J. ; Mantooth, A. "A Comparison of Silicon and Silicon Carbide MOSFET Switching Characteristics", IEEE Region 5 Technical Conference, pp. 273-377, April 2007.

[8] Tiefu Zhao ; Jun Wang ; Huang, A.Q. ; Agarwal, A. "Comparisons of SiC MOSFET and Si IGBT Based Motor Drive Systems", Industry Applications Conference, 2007. 42nd IAS Annual Meeting. Conference Record of the 2007 IEEE, pp. 331-335, Sept. 2007.

[9] De, D. ; Castellazzi, A. ; Lopez-Arevalo, S. ; Lamantia, A." SiC MOSFET based avionic power supply", Power Electronics, Machines and Drives (PEMD 2014), 7th IET International Conference on, pp. 1-6, April 2014.

[10] P. W. Wheeler, "The more electric aircraft: Why aerospace needs power electronics?" Power Electronics and Applications, 2009. EPE '09. 13th European Conference on, pp. 1-30, Sept. 2009.

[11] Cree, CPM2-1200-0040B Silicon Carbide Power MOSFET Datasheet, Rev B, 2014.

[12] Cree, CPW4-1200S020B Silicon Carbide Schottky Diode Chip Datasheet, 2011.

[13] Microsemi, Military ProASIC3 Low-Power Flash FPGAs Datasheet, Revision 5, Sept. 2014.

[14] Microsemi, UG0478 User Guide IGLOO2 FPGA Evaluation Kit, Revision 4.1, 2017.

[15] Infineon, 1EDI EiceDRIVER™ Compact Datasheet, Rev. 2.0, 2014.

[16] Texas Instruments, ISO5852S High-CMTI 2.5-A and 5-A Reinforced Isolated IGBT, MOSFET Gate Driver Datasheet, August 2015, Revised January 2017.